Effects of Passives on the Performance of an Axial Flow Compressor

S.M.Swamy[1] and G.P.Prasada Reddy[2]

[1]*Asst.Professor. Department of Mechanical Engineering, G.Narayanamma Institute of Technology and Sciences, shaikpet, Hyderabad-104*
[2]*Professor, Department of Mechanical Engineering, G.Narayanamma Institute of Technology and Sciences, shaikpet, Hyderabad-104*
Corresponding Auther: S.M.Swamy

Abstract: *The flow field at the rotor exit of an axial flow compressor for different tip geometries and for different flow coefficients is measured by using simple passive means in the present experimental study. The following configurations are tested: (i) basic rotor configuration without any passive means (ii) rotor with partial shroud (iii) rotor with partial shroud and turbulence generator, TG placed on the casing at the leading edge of the rotor blade. The turbulence generators are made of velcro tape. From the steady state measurements, the performance of rotor with PS and TG is found to be the best. Both the rotors with partial shrouds and turbulence generators have stalled at a higher flow coefficient compared to that of rotor without passive means. From the periodic flow measurements, it is concluded that the low velocity region near the tip section is considerably reduced with the partial shrouds use. The extent of this low velocity region for both rotor with basic and rotor with partial shroud, increases with decreasing flow coefficient due to increased stage loading with this low momentum fluid has moved inward of the annulus and towards the pressure side as the flow coefficient decreases. The improved performance of the rotor with passive means is attributed to the energization of the casing wall boundary layer at the rotor inlet, due to vortexes generated by TG.*
Keywords: Compressor, rotor with partial shroud, rotor with turbulence generator.

Nomenclature:
d   diameter, m
h   rotor blade chord, mm
PS   partial shrouds
n   impeller rotational speed, rpm
p   pressure, N/m^2
r   radius, m
s   blade spacing, mm
SS   suction surface
t   tip clearance, mm
TG   turbulence generator placed at the rotor
       leading edge
U   peripheral velocity, m/s
V   volume flow rate, m^3/s
α absolute flow angle, deg.;
       stator blade angle, deg.
β rotor blade angle, deg.
ψ pressure coefficient,
ϕ flow coefficient,
γ stagger angle, deg.
ρ density, kg/m^3
τ tip clearance as percentage of chord, t/Ch_t
      x 100

Subscripts

1   rotor inlet
2   rotor exit
3   stator exit
b   blade
c   casing
h   hub
o   total
R   rotor
S   stator
s   static
t   tip

I.   Introduction:

Axial flow compressors have a wide range of applications especially for power plants and industrial applications compared to centrifugal compressors. Due to bulky construction, large frontal area causing higher drag and lower power to weight ratio of centrifugal compressors, axial flow compressors are gaining high popularity over the centrifugal compressors. Efficiency is probably the most important performance parameter for turbomachines. But there are various losses associated with turbomachines that tend to reduce the performance of turbomachines. Tip leakage loss plays a major role in reducing the performance because of less knowledge of flow field in the tip region. Most of the earlier research was confined to understand this flow field in large-aspect-ratio rotors (Hunter and Cumpsty [1], Lakshminarayana et al. [2], Inoue and Kuroumaru [3], and Lakshminarayana et al. [4]). A comprehensive review of the investigations on the turbomachinery tip clearance effects is given by Peacock [5]. These techniques generally involve some form of casing treatment near the rotor tip for the purpose of delaying rotor tip stall or reducing the detrimental effects resulting from excessive tip clearance. These techniques are casing treatment [6], vortex generators on the casing wall and rotor blades [7], recessing the casing over the rotor tips [8], recessed vane casing [9], and shrouding of the blades. In addition many active techniques are used to control tip clearance flows. Some of these are air injection [10] and plasma actuation [11]. Partial shrouds may provide a significant aerodynamic performance gain. This gain is expected because the leakage flow, initiated near the leading edge on the blade pressure surface, would travel a longer distance over the width of the shroud during which it is forced further downstream. On emerging from the tip clearance, leakage flow interaction with the passage flow near the tip suction surface takes place further downstream where its harmful effects are reduced. Patel [12] conducted tests with and without partial shrouds on the rotor blades of a single stage axial gas generator turbine at different values of tip clearance. He observed 1.2-point improvement in total efficiency with partial shrouds. But he found that the sensitivity of performance to the tip clearance remains unaltered by partial shrouds. Ishida et al. [13] found that a partial shroud attached to the tip of a rotor blade of a centrifugal blower improved its performance. Corsini et al. [14] had carried out extensive investigations on axial flow fans with partial shrouds with the objective of reducing noise. Akturk and Camci [15] measured three-dimensional mean flow near the tip of a ducted axial fan rotor using a stereoscopic particle image velocimeter.

The present paper reports results of an experimental investigation, where improved performance and operating range of a low aspect ratio axial flow compressor are obtained by using a similar technique. In this technique, the turbulence generator (velcro tape) is placed upstream of the rotor leading edge. Thus this technique can be used even when the tip clearance is small.

II.   Motivation and Objective

The flow in the axial flow compressors is very complex and highly three-dimensional. The flow at the exit of the rotor is highly non uniform in both axial and circumferential directions and highly turbulent. Axial flow compressors have higher loading levels, higher efficiency, better stability, and vibrational characteristics. They are more distortion tolerant due to larger chords of the rotor blades. Such compressors find applications in the rear stages of multistage axial compressors in aircraft gas turbine engines and for ventilation purposes.

There are relatively few investigations on axial compressor aerodynamics in spite of their importance. Because of large values of relative tip clearance (tip clearance/blade span), the clearance losses in axial flow compressors are expected to be large. The objective of the present research is to investigate the effectiveness of the partial shrouds attached to the tip of the rotor blades of axial-flow compressor to reduce the tip clearance losses.

III.   Experimental Facility and Instrumentation

The present investigation is carried out on the axial flow compressor. A schematic layout of the test facility is shown in Fig. 1. Partial Shroud: The configurations studied are rotor without partial shroud, rotor with partial shroud, and rotor with partial shroud turbulence generator, to permit small amount of leakage flow to leak over the tip. The partial shroud is made from a 0.2mm thick stainless steel sheet. The sheet is rolled to the rotor tip diameter, and then the profiles matching the required partial shroud are cut. These profiled shrouds are pasted onto the tip of the blade using a very thin layer of Araldite. This method seemed to be satisfactory as no partial shroud came off with the rotor operating at the design speed of 1450 rpm. Also, no vibrations of the partial shrouds were observed from the stroboscope visualizations. Care is taken so that there are no burrs at the edges of the shroud, which otherwise would cause frictional losses. The shape of the shroud is chosen as aerofoil corresponding to the tip section, but with 11% maximum thickness, which is equal to twice the maximum thickness of the rotor blade tip section. The partial shroud is extended about 5mm downstream of the rotor blade leading edge and about 5mm upstream of the rotor blade trailing edge. The rotor tip diameter, d_t is 0.580 m and hub diameter is d_h of 0.450 m, giving a hub/tip ratio of 0.77. Further details are the facilities are given in Table 1. The rotor tip clearance is 1.5 mm giving a relative tip clearance of $\tau = 1.1\%$. Details of the rotor blades are given in Table 2. The volume flow rate of air through the rotor is measured using the calibrated inlet nozzle. The speed of the rotor is measured with a non-contact type electronic tachometer with an accuracy of ± 1 rpm. The casing has provision to mount traversing mechanisms at three axial locations S_1, S_2 and S_3, at the inlet and exit of the rotor and exit of stator respectively. Static pressure tappings are provided on the casing at inlet and exit of the rotor and exit of the stator. Turbulence generators are used in the experiment as a tripping device for the generation of turbulent boundary layers. A turbulence generator (TG) is pasted on the casing wall upstream of the rotor. A turbulence generator (TG) is made of an approximately 2 mm thick Velcro tape material of 1820 mm long and 25 mm width. Sketches of the Velcro tape geometries and PS are shown in Fig. 2. The rotor exit flow using a precalibrated five hole probe is traversed in the radial direction, and measurements are taken at twenty radial locations for four flow coefficients, namely, $\varphi = 0.36$, near stall flow coefficient, $\varphi = 0.48$, below design flow coefficient, $\varphi = 0.55$, near design flow coefficient, and $\varphi = 0.64$, near maximum flow coefficient. A scanning box (Model FCO91-3) and micromanometer (Model FCO12), manufactured by M/s. Furness Control Ltd., UK, are used to measure the pressure sensed by the pressure probes. The scanning box contained 20 valves which are numbered sequentially. The pressures to be measured are connected to the numbered inputs. Pressure inputs are read in sequence by using the micromanometer. The micromanometer is a sensitive differential pressure measuring unit, capable of reading air pressures from 0.01 mm to 200 mm WG. It would respond to pressure inputs up to 50 Hz. But the time constant potentiometer can be used to average the pressure fluctuations. The accuracy of the measured pressure is within $\pm$ 0.01 mm WG.

IV.   Results and Discussion

The results of the present experimental investigations are presented and interpreted in the following sections. First the rotor performance, in terms of static pressure coefficient across the rotor tip, derived from casing wall static pressures measured before and after the rotor for the three configurations is presented. The results are presented for three configurations including basic configuration and at four flow coefficients, viz. $\phi = 0.64$ (above design flow coefficient), 0.55 (design flow coefficient), 0.48 (below design flow coefficient), and 0.36 (stall flow coefficient). The three configurations studied are (i) rotor without passive means, tip clearance $\tau = 1.1\%$, (ii) rotor with partial shrouds (PS), tip clearance $\tau = 1.1\%$ and (iii) rotor with partial shrouds (PS) and turbulence generator (TG) upstream of the rotor leading edge, tip clearance $\tau = 1.1\%$. The total and static pressures are non-dimensionalised by the dynamic head derived from U_C. These non-dimensional values are presented against the percent span from hub.

4.1. Performance Characteristics:

The performance characteristics of the axial flow compressor rotor for three configurations are shown in Fig. 4. The abscissa of this figure represents flow coefficient, whereas, ordinate represents the static pressure rise coefficient across the rotor at the casing. It can be seen that Configuration 3 (rotor with PS and TG) shows increased static pressure rise across the rotor at casing compared to other configurations. The reason is that TG energises the casing wall boundary layer. Stall occurs at $\phi = 0.44$, compared to Configuration 1 (Basic configuration), for which stall occurs at $\phi = 0.464$. The most probable reason for this may be due to the large disturbances caused by the TG right at the rotor leading edge. It is also observed that with PS, stall occurs at a higher flow coefficient.

4.2. Rotor Exit Flow Measurements:

Total pressure coefficient,(ψ_{02}): The distribution of total pressure coefficient at the rotor exit for three configurations and four flow coefficients is shown in Fig.5. From the figure it is clearly observed that, there is substantial increase in total pressure for the rotor with partial shroud compared to that of rotor free vortex design of the rotor is confirmed by the total pressure distribution at $\phi = 0.55$, which is almost constant outside the annulus wall boundary layers. It is clearly shows that for $\phi = 0.64$, and 0.48, there is a definite increase in total pressure over a large radial extent for the rotor with the configuration of PS and TG compared to configurations of rotor with PS. But for $\phi = 0.36$ rotor with PS show more total pressure rise as compared to rotor with PS and TG but with reduced stable operating range as stall occurs at higher flow coefficients, whereas, at design flow coefficient $\phi = 0.55$ both these configurations show almost same total pressure rise.

Static pressure coefficient,(ψ_{S2}): The distribution of static pressure coefficient for the four flow coefficients and three configurations, at the rotor exit is shown in Fig. 6. From figure it is shows that for basic configuration as well as for other configurations static pressure rise remains almost constant. For $\phi = 0.64$, Configuration 2 of rotor i.e. rotor with partial shrouds shows large fluctuations in static pressure from hub to tip due to use of partial shrouds.

Careful study of this figure observed that static pressure coefficient is more for basic configuration and reduced for rotor with partial shroud at $\phi = 0.64$. This is due to leakage flow acts in opposite direction of secondary flows, but partial shroud restricts leakage flow, reducing the scope of decreasing secondary flows and losses, the static pressure rise is not high even though for these flow coefficients (except for $\phi = 0.48$) total pressure is high.

Total Pressure Loss Coefficient, (ψ_{loss2}): The spanwise variation of total pressure loss coefficient for the four flow coefficients and for the three configurations at the rotor exit is shown in Figure 7. The total pressure loss coefficient is defined as follows:

$$\psi_{loss2} = 2(\rho U_2 C_{2u} - Po_2)/\rho U^2 c, \qquad (1)$$

where P_{o2} is total pressure at rotor exit, Pa, U_2 is rotor speed, m/s, Uc is rotor speed corresponding to the casing radius, m/s, and C_{2u} is tangential velocity at the rotor exit, m/s. It can be seen that the losses are high in the annulus wall boundary layers and loss coefficient increases in the tip regions as the loading increases. The loss coefficient is minimum at the design flow coefficient. For flow coefficients, 0.64, 0.55, and 0.48, the loss coefficient is lowest for rotor with passive means.

Absolute velocity,(C_2): The span wise distribution of absolute velocity for the four flow coefficients and three configurations is shown in Fig. 9. It can be seen from the figure that the absolute velocity almost remains constant at design flow coefficient and above the design flow coefficient ($\phi = 0.64$ and 0.55). Also it is observed that these flow coefficients show the same absolute velocity for shrouded cases. Careful study of this figure shows that basic configuration give lower absolute velocity for flow coefficient at, above and just below design flow coefficient.

Absolute flow angle, (α_2): The span wise variation of absolute flow angle for the four flow coefficient and for the three configurations at the rotor exit is shown in Fig. 10. The angles shown are with respect to tangential direction. For $\phi = 0.64$, 0.55 and 0.36, from Fig. 10, it is clear that for Configuration 3 (rotor with PS and TG) lower absolute flow angles have been observed for the most of the span. With almost same axial velocity and decrease in absolute flow angle means increase in tangential velocity, which in turn causes more losses. But lower absolute flow angle for the same axial velocity indicates higher absolute velocity with Configuration 3 (rotor with PS and TG) compared to Configuration 2 (rotor with PS only) and thereby higher total pressure. So the incidence angle at stator inlet for the configuration is higher.

Mass averaged flow parameters: Figure 8 shows the variation of mass averaged values of total pressure rise coefficient ($\overline{\psi}_O$) and static pressure rise coefficient ($\overline{\psi}_S$) with flow coefficient. This figure clearly shows improvement in $\overline{\psi}_O$ and $\overline{\psi}_S$ for rotor (with PS and TG) compared to rotor (with PS only). Due to vortices generated by TG upstream of rotor, casing wall boundary layer is energised, which cause delay in boundary layer separation consequently losses are reduced. Configuration 3 (rotor with PS and TG) shows improved pressure rise than that of Configuration 1. But static pressure rise for this configuration in tip region is slightly less than that of Configuration 2. This configuration shows early stalling compared to Configuration 3. This early stalling may be due to boundary layer separation due to high adverse pressure gradient at this flow coefficient. It can be inferred that though the partial shrouds increase peak pressure rise, stall occurs at higher flow coefficient, reducing the useful operating range. From figure 8, it can be seen that there is a definite increase in static pressure for rotor with passive means configuration for flow coefficients of 0.64, 0.55, and 0.48 at the rotor exit. In case of rotor with partial shroud, though the total pressure is higher than that of rotor with basic, static pressure is less at the rotor exit, at $\phi = 0.36$, the static pressure is maximum for rotor with basic.

V.   Conclusions

1. From the performance of rotor determined from the wall static pressures measured on the casing before and after the rotor tip, Configuration 3 (rotor with PS and TG) stalls at a lower flow coefficient compared to other configurations. Also the static pressure rise coefficient is slightly higher compared to that for other configurations. Configuration 2 (rotor with PS) and Configuration 1 (rotor with basic) gave poor performance, i.e. reduced operating range and reduced static pressure rise coefficient over the entire operating range.

2. Turbulence generator (TG) causes the casing wall boundary layer to get energized which in turn causes delay in boundary layer separation. Hence losses are less and better stable operating range is achieved. Although, measurements at the rotor inlet cannot taken for Configuration 3, due to the disturbed flow because of TG, it is believed that the boundary layer at the rotor is turbulent even at near and below flow coefficient, $\phi = 0.36$.

3. The mass averaged total pressure rise coefficient and static pressure rise coefficient show improved for Configuration 3 (rotor with PS and TG) compared to other two configurations. For a proper comparison, only the performances of Configurations 2 and 3 must be compared, as both would include the detrimental effects of modified partial shrouds.

   The present experimental investigation is an initial attempt to improve performance of an axial-flow compressor fan rotor using a fairly rough tip modification. Although performance of the rotor is improved at and above design conditions by means of the perforated partial shroud, stall margin is reduced. The most probable reason is the use of partial shroud of large width. The maximum width of the partial shroud is 11% of chord, while the maximum thickness of the blade at the tip is 5.5%. It can be anticipated that per-formance and stall margin of the rotor may be improved by using improved partial shrouds, such as partial shrouds on pressure side only, partial shrouds having shorter chord than the blade at the tip, profiled partial shrouds, perforated par-tial shrouds, straight and inclined squealer tips, and so forth. Such successful attempts are reported in [14–17].

References

[1].   I. H. Hunter and N. A. Cumpsty, "Casing wall boundary layer development through an isolated compressor rotor," ASME Journal of Engineering for Power, vol. 104, no. 4, pp. 805–817, 1982.

[2].   B. Lakshminarayana, M. Pouagare, and R. Davino, "Threedimensional flow field in the tip region of a compressor rotor passage— part I: mean velocity profiles and annulus wall boundary layer," ASME Journal of Engineering for Power, vol. 104, no. 3, pp. 760– 771, 1982.

[3].   M. Inoue and M. Kuroumaru, "Structure of tip clearance flow in an isolated axial compressor rotor," ASME paper number 88-GT-251, 1988.

[4].   B. Lakshminarayana,M. Zaccaria, and B.Marathe, "The structure of tip clearance flow in axial flow compressors," ASME Journal of Turbomachinery, vol. 117, no. 3, pp. 336–347, 1995.

[5].   R. E. Peacock, "Turbomachinery tip gap aerodynamics," in Proceedings of the 9th International Symposium on Air Breathing Engines, pp. 549–559, Athens, Greece, September 1989.

[6].   H. Takata and Y. Tsukuda, "Stall margin improvement by casing treatment- its mechanism and effectiveness," ASME Journal of Engineering for Power, vol. 99, no. 1, pp. 121–133, 1977.

[7].   C. H. Law, A. J. Wennerstrom, and W. A. Buzzell, "The use of vortex generators as inexpensive compressor casing treatment," SAE Paper, no. 760925, 1976.

[8].   D. C.Wisler and B. F. Beacher, "Improved compressor performance using recessed clearance (trenches)," AIAA Journal of Propulsion and Power, vol. 5, no. 4, pp. 469–475, 1989.

[9].   S. D. Hill, R. L. Elder, and A. B. McKenzie, "Application of casing treatment to an industrial axial-flow fan," Proceedings of the Institution of Mechanical Engineers, Part A, vol. 212, no. 4, pp. 225–233, 1998.

[10].   H. Khaleghi and J. A. Teixeira, "Numerical study of discrete tip injection in a transonic axial compressor," in Proceedings of the ASME Turbo Expo Turbine Technical Conference, no. GT2010- 23608, pp. 525–535, Glasgow, UK, June 2010.

[11].   J. Giridhar, R. C. Murray, K. Essenhigh et al., "Control of tipclearance flow in a low speed axial compressor rotor with plasma actuation," in Proceedings of the ASME Turbo Expo Turbine Technical Conference, no. GT2010-22345, pp. 161–172, Glasgow, UK, June 2010.

[12].   K. V. Patel, "Research on a high work axial gas generator turbine," SAE Paper, no. 800618, 1980.

[13].   M. Ishida, H. Ueki, and Y. Senoo, "Effect of blade tip configuration on tip clearance loss of a centrifugal impeller," ASME Journal of Turbomachinery, vol. 112, no. 1, pp. 14–18, 1990.

[14].   A. Corsini, F. Rispoli, and A. G. Sheard, "Shaping of tip endplate to control leakage vortex swirl in axial flow fans," ASME Journal of Turbomachinery, vol. 132, no. 3, pp. 1–9, 2010.

[15].   A. Akturk and C. Camci, "Axial flow fan tip leakage flow control using tip platform extensions," ASME Journal of Fluids Engineering, vol. 132, no. 5, pp. 0511091–05110910, 2010.

[16].   A. Akturk and C. Camci, "Tip clearance investigation of a ducted fan used in VTOL UAVs, part 1: baseline experiments and computational validation," in Proceedings of the ASME Turbo Expo Turbine Technical Conference, no. GT2011-46356,Vancouver, Canada, June 2011.

[17].   A. Akturk and C. Camci, "Tip clearance investigation of a ducted fan used in VTOL UAVs, part 2: novel treatments via computational design and their experimental validation," in Proceedings of the ASME Turbo Expo Turbine Technical Conference, no. GT2011-46359, Vancouver, Canada, June 2011

Table 1 Details of the Low Aspect Ratio Axial Flow Compressor

Design volume flow, V	= 3.5 m^3/s	Speed, n	= 1450 rpm
Specific work, W	= 650 m^2/s^2	Free vortex design	
Rotor hub diameter, d_h	= 450 mm	Rotor tip diameter, d_t	= 580 mm
Number of rotor blades, Z_R	= 14	NACA 0008 type FRP rotor blades	
Number of stator blades, Z_S	= 13	Circular arc sheet metal stator blades	
Rotor aspect ratio, AR_R	= 0.5	Stator aspect ratio, AR_S	= 0.47

Rotor tip clearance, t (t/Ch $*$ 100%) = 1.5mm (1.1%)
Shape number, Nsh = n$\sqrt{V}$/(60W$^{0.75}$) = 0.30

Table 2 Details of Rotor Blades

Rotor Blades								
Sl. No.	D mm	Radius, ratio, R	β_{1b} Deg.	β_{2b} Deg.	γ Deg.	S (mm)	s/Ch	Ch_R mm
1	450	0.773	35.2	59.5	55.0	101.0	0.743	136
2	477	0.797	33.6	55.7	52.9	104.1	0.789	136
3	505	0.819	32.2	52.3	48.8	107.0	0.834	136
4	532	0.843	30.8	49.1	45.9	110.2	0.878	136
5	560	0.869	29.5	46.2	43.3	113.3	0.924	136
6	580	0.891	28.4	43.5	40.7	116.5	0.962	136

Table 3 Stall Flow Coefficient for Different Configurations

Configuration No.	Config. 1	Config. 2	Config. 3
ϕ_{stall}	0.465	0.475	0.441
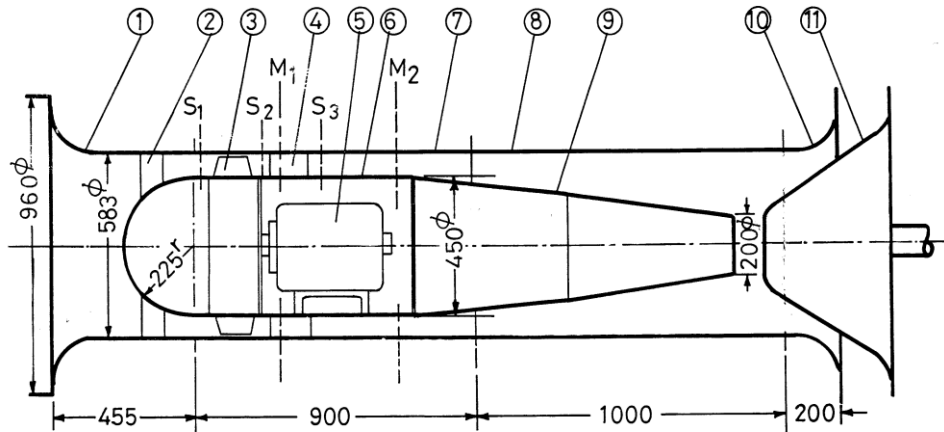
1. Inlet Nozzle   2. Radial Supports for Hub Nose Cone   3. Rotor 4. Stator   5. A.C. Motor 6. Motor Housing 7. Casing   8. Exit Duct 9. Conical Hub   10. Exit Nozzle   11. Throttle Cone
M1 and M2: Location of Stay Rods for Motor Housing S1, S2 and S3: Traverse Stations for Probes
All Dimensions in Millimeters
Fig.1 Schematic Lay Out of Flow Compressor Facility

Configurations Tested

Figure.2. Velcro tape geometries and Partial shroud attached on the rotor

Rotor (w/o ps)
Rotor (with ps)
Rotor (with passive means)
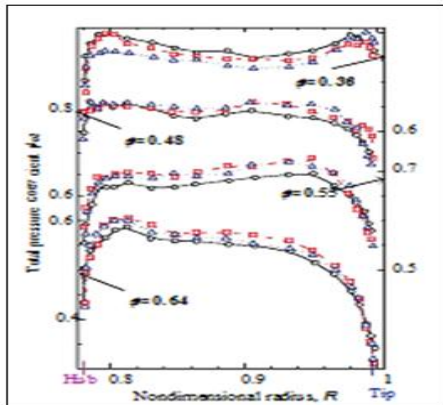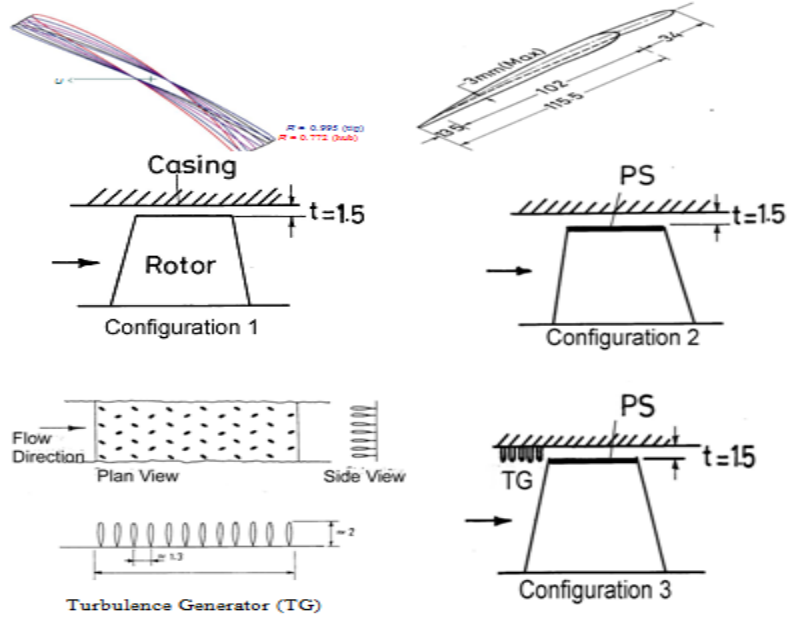
Figure 4: Performance Characteristics of Axial flow Rotor with and without passive Means.
Figure 5: Radial distribution of total pressure coefficient at the rotor exit.

Rotor (w/o ps)
Rotor (with ps)
Rotor (with passive means)
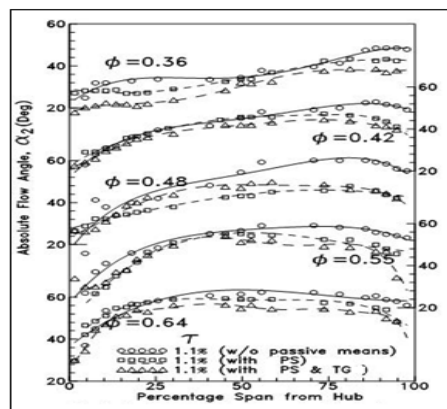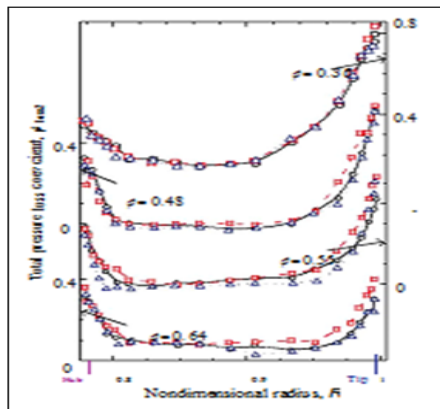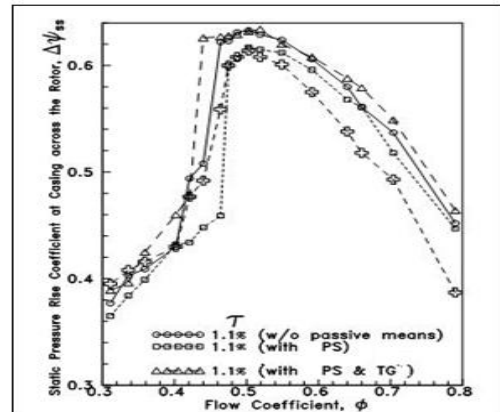
Figure 7: Radial distribution of total pressure loss coefficient
at the rotor exit.
Figure 9: Radial Distribution of Absolute velocity of Rotor Exit.
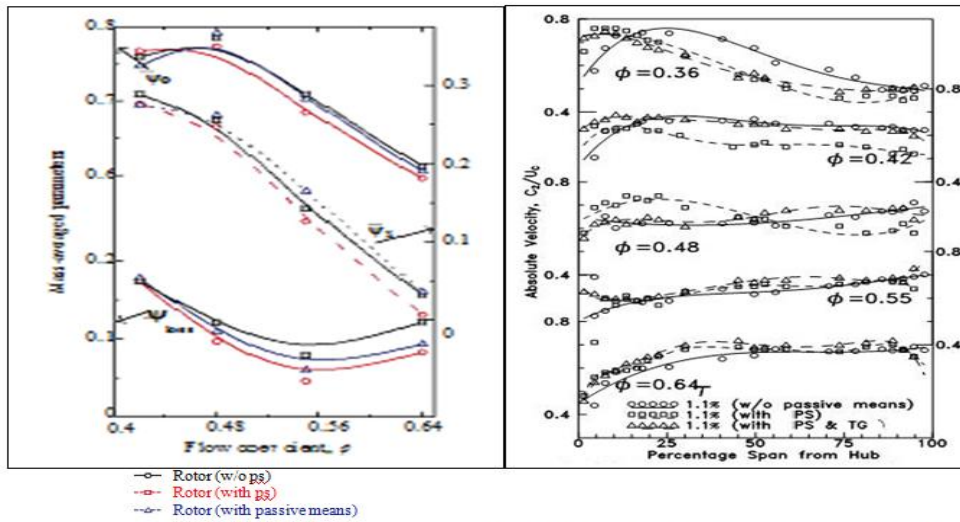
Figure 8: Mass-averaged performance of the Axial- Flow Compressor.
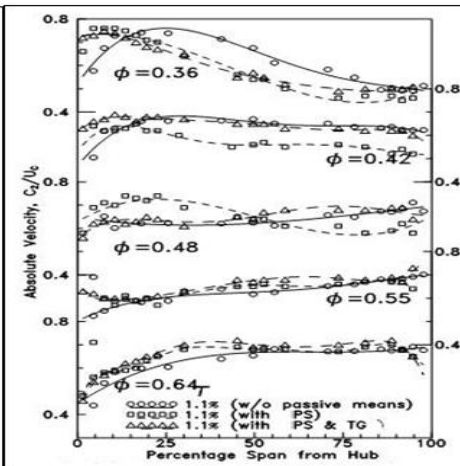
Figure 10: Radial Distribution of Absolute Flow Angle of Rotor Exit.
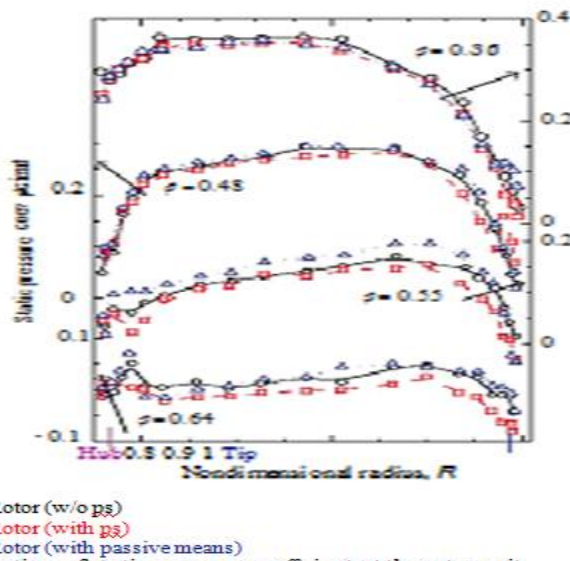
Figure 6: Radial distribution of static pressure coefficient at the rotor exit

S.M.Swamy "Effects of Passives on the Performance of an Axial Flow Compressor "International Journal of Engineering Science Invention (IJESI), vol. 07, no. 06, 2018, pp 72-79